

Achievements of Aerial Prediction of Earthquake and Rain Induced Rapid and Long-Travelling Flow Phenomena (APERITIF) Project

Kyoji SASSA, Hiroshi FUKUOKA, Tatsuo SEKIGUCHI*, Hiromu MORIWAKI **, and
Hirotaka OCHIAI ***

* Geographical Survey Institute, Ministry of Land, Infrastructure and Transport

** National Institute for Earth Science and Disaster Prevention

*** Forestry and Forest Product Research Institute

Synopsis

Risk evaluation for earthquake induced rapid and long-travel landslides in densely populated urban areas is currently the most important disaster mitigation task in landslide-threatened areas throughout the world. The major research achievements of the Aerial Prediction of Earthquake and Rain Induced Rapid and Long-Travelling Flow Phenomena (APERITIF) project which was coordinated by Sassa, is introduced in this paper; (1) Detection of landslide prone slope using airborne laser scanner, (2) Full-scale landslide flume test using artificial rainfall instrument, (3) Landslide triggering experiment on natural slope by artificial rainfall, (4) Landslide risk evaluation and hazard zoning in urban development areas. Test site of (4) is the Tama residential area near Tokyo. A set of field and laboratory investigations including laser scanner, geological drilling and ring shear tests showed that there was a risk of sliding surface liquefaction for both sites. A geotechnical computer simulation (Rapid/LS) using the quantitative data obtained in the study allowed urban landslide hazard zoning to be made, at individual street level.

Keywords: risk evaluation, hazard zoning, earthquake-induced landslides, fluidization, Airborne laser scanning, full-scale model experiment, natural slope, pore-water pressure, sliding surface formation, undrained ring-shear tests, numerical simulation

1. Introduction

The protection of life and property from natural disasters is indispensable in creating an environment for society that ensures safety and satisfaction for its people. The national imperative towards safety and satisfaction is increasing in countries suffering from natural disasters. Landslide disasters are generally less recognized in the statistics of the United Nations and many governments than events such as earthquakes, volcanic eruption and meteorological disasters, because most landslide disasters often occur in association with earthquakes, typhoons or hurricanes and volcanic activities and are

thus classified as earthquake disasters, meteorological disasters or volcanic disasters. Nonetheless, the total number of deaths in Japan owing to landslides during the past 30 years, from 1967-1998, was 3,152, while the number owing to earthquakes was 6,254, including the 1995 Kobe earthquake. Taking an even longer period, landslide disasters have caused a greater number of deaths than earthquakes, and indeed the number of deaths from landslides far exceeds that from earthquakes. Though landslide disasters are not as sensational as earthquake disasters, the former have the same level of social significance.

Some landslides move slowly, on the order of

centimeters per year, whilst others move at meters per day, and still others move rapidly at velocities over 50 m/s: high velocities from which people cannot always escape. Within this field of rapid landslides, some move only a short distance, whereas others travel long distances. As illustrated in Fig. 1, landslides can be classified into four types according to velocity and travel distance. The first type consists of landslides that are rapid and short-moving, including most types of debris slides and rock falls. In most countries these types of landslides are the most frequent, although they are usually small in scale. This type of landslide impacts people in the mountainous areas of the world, and the associated risk is obvious, because of the steepness of the slopes and the proximity of dwellings to the steep slopes. The second type consists of reactivated landslides that move slowly for a short distance. Often homes and farmlands are constructed on such landslides. The third type of landslide is slow and long-travel failures such as earth flows. These latter two types do not threaten the lives of people because it is often possible to evacuate people from the impacted area quickly. The fourth type are rapid and long-travel landslides which are clearly the most dangerous since the rapid motion does not allow for evacuation, and a great impact force is typically generated which can destroy houses and disastrously affect a large area. Often the danger is not obvious. Houses that have been constructed away from steep slopes, or often on gentle slopes can be destroyed by this phenomenon. The Tsukidate landslide reported by Fukuoka et al. (2004) is a typical example, as it moved from a gentle slope of only 10° and traveled a long distance at a speed of several meters per second.

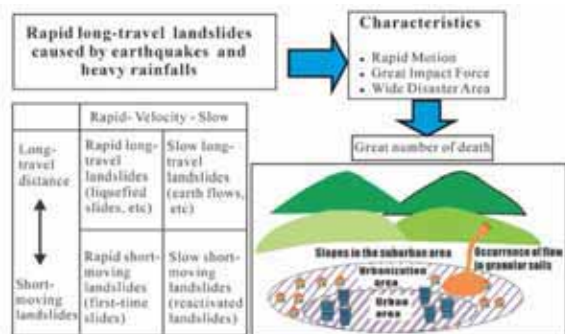


Fig. 1 Types of landslides in terms of velocities and travel distances

What is the definition of a long-travel landslide? Long travel distance means that the travel distance is beyond the normal expectations of most people.

Therefore, it is not always likened to the absolute value of travel distance. Fig 2 presents what is the expected travel distance of landslides. The long or short travel distance is not the function of travel distance itself, but rather the function of mobility. The index of mobility is expressed by the apparent friction (H/L) and the apparent friction angle (α) as shown in Fig. 2a. Fig. 2b presents the statistics of H/L for the period of 1972 – 1995 for landslides in Japan. In these statistics, most landslides (more than 97%) had an H/L value of more than 0.5 or an apparent friction angle of more than 26°. High values of H/L indicate that the landslide masses moved onto a flat area and subsequently lost energy, or were often blocked by walls or houses. Less than 3% showed high mobility in the debris slides and falls in Japan (locally called Gake-kuzure, steep slope failures); 3% can be within error limits, or a negligible rate in political decisions. However, this small number is still very important.

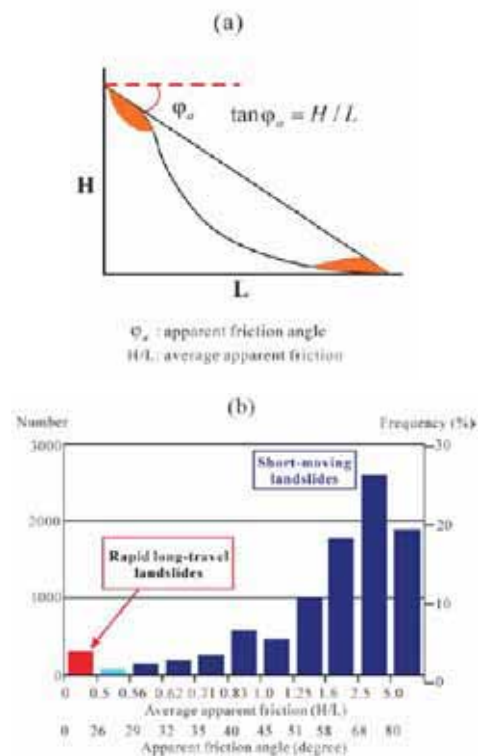


Fig. 2a,b Index to express mobility and frequency of debris slides and falls in Japan. (a) Illustration of apparent friction angle. (b) Statistical chart of life loss (by the Ministry of Construction of Japan, 1997).

In Fig. 3, some examples of recent major landslide disasters are listed in terms of fatalities and the apparent friction angles, mostly in Japan, but also including recent large disasters in other countries. It should be understood that most of these had high mobility, with apparent

friction angles of around 10° or even higher. However, all of them had apparent friction angles of less than 20° , which is below the 30° that is near the friction angle of sandy materials mobilized during motion in the apparent friction angle. Therefore, it is clear that large landslide disasters have been caused by landslides of exceptionally high mobility.

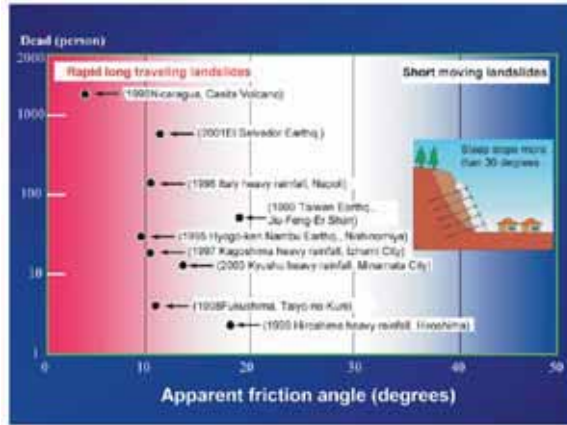


Fig. 3 Examples of recent catastrophic landslide disasters in Japan and other countries

Both Fig. 2 and Fig. 3 visualize the significance of research on rapid long-travel landslides with high mobility, although the physical occurrences are very limited. A project called the Areal Prediction of Earthquake and Rain-Induced Rapid and Long-Travelling Flow Phenomena (APERITIF) was originally proposed for a Special Coordinating Fund for Promoting Science and Technology of the Ministry of Education, Culture, Sports, Science and Technology of Japan (MEXT) under this understanding. It was adopted as a project in the group category of Social Infrastructure for a 3-year period from 2001 to the end of March 2004. It was named as “APERIF” (Aerial Prediction of Earthquake and Rain Induced Flow Phenomena). After March 2004, its achievements received rather high evaluation from the funding agency.

After that, this project was approved as one of projects of the International Programme on Landslides (IPL M101 = APERITIF) coordinated by the International Consortium on Landslides (ICL) when it was established in 2002 for further worldwide development of APERIF.

The APERITIF project consists of (1) researching the mechanism of rapid and long-traveling flow phenomena, (2) development of micro-topographical survey technology to extract dangerous slopes, (3) development

of technology to assess hazardous area, and (4) integrated research for urban landslide zoning. Research topic (1) includes the development of dynamic loading ring shear apparatus with a transparent shear box reported by Sassa et al. (2004a). Topic (2) includes the airborne laser scanner technology to measure micro-topography under forests (Sekiguchi et al., 2004), while topic (3) includes large-scale (similar to the real scale of landslides) flume tests to reproduce landslides (Moriwaki et al., 2004), and a field experiment to reproduce a rapid and long-travel flow phenomena by artificial rainfall onto a natural slope with various monitoring equipment (Ochiai et al., 2004), and topic (4) includes risk evaluation of rapid and long-travel flow phenomena which may be triggered by sliding surface liquefaction and the trial urban landslide zoning (Sassa et al., 2004c). This paper contains above major research achievement from this project.

The development of reliable landslide risk evaluation and precise landslide zoning technology in urban areas and locations of high societal value is currently a pressing need. Much more research has yet to be completed. However, the establishment of this technology is now possible because necessary key technology is now in our hands. We can approach and directly observe the source area and the sliding surface of landslides, and it is possible to measure the necessary mechanical parameters, such that we can stabilize a dangerous slope if the danger is identified with a high reliability, or we can avoid the landslide risk by relocation of houses and facilities. The United Nations World Conference on Disaster Reduction was organized in Kobe, Japan, in January 2005, 10 years after the 1995 Kobe earthquake disaster, which included the Nikawa rapid and long-travel landslide that killed 34 persons. Authors believe the landslide research community is sure to succeed in its steady progress, both in increasing the reliability of risk evaluation, and towards preparedness for such dangerous landslides in the coming decade of 2005 – 2015 across the world, under close collaboration with the supporting organizations of ICL: four United Nations bodies (UNESCO, WMO, FAO, UN/ISDR), IUGS (International Union of Geological Sciences), and the Governments of Japan, USA and others. It will be an important contribution to the United Nations International Strategy for Disaster Reduction (UN/ISDR). In the following sections, major achievements of APERIF projects are introduced.

2. Mapping of micro topography using airborne laser scanning

In order to understand disastrous landslides it is important to identify the geometrical and geomorphological conditions of slopes in which the landslides have previously occurred. Photogrammetry has frequently been used for such measurements. In addition, it has become possible to use a method called airborne laser scanning for detailed three-dimensional measurements.



Fig. 4 Measuring principle of airborne laser scanning

Airborne laser scanning has recently been used in terms of landslide identification (Aleotti et al., 2000; Hasegawa and Okamatsu, 2001; Sato et al., 2002; Sekiguchi et al., 2003). It is expected that airborne laser scanning will enhance not only high-precision mapping but, also landform analysis (Ackermann, 1999; Wehr and Lohr, 1999; Masaharu et al., 2001). Using the acquired data, high-precision topographic maps, inclination classification maps and shading maps can be produced more efficiently. Furthermore, through micro topographic mapping, analysis for landslide simulation and unstable slope identification may be actively performed (Sekiguchi et al., 2003). The purpose of this study is to show an example of the micro topography mapping of hilly terrain using airborne laser scanning data in the Tama Hills near Tokyo, Japan. The study area was Tama Hills are located near the boundary between the western Kanto Mountains and the Kanto Plain, southwest of Tokyo, Japan.

2.1. Data preparation

(1) Airborne laser scanning

Airborne laser scanning uses an active sensor that measures the distance from the sensor to the ground where the laser beam is reflected (Fig. 4). Aircraft positions are calculated using a combination of Global Positioning System (GPS) data, both on the aircraft and on the ground, aircraft acceleration and three-axial attitude data measured by an Inertial Measurement Unit (IMU). Furthermore, the direction data of the laser beams are measured by a sensor onboard the aircraft. These data are combined to calculate the three-dimensional position (X, Y, Z) on the ground.

In this study, the measurement specifications were as follows using the laser instrument, EnerQuest RAMS system:

laser wavelength:	1064 nm;
pulse rate:	24000 Hz;
scanning frequency:	24 Hz;
flying altitude:	normally above 2600m;
flight speed:	203.7 km/h;
swath width:	881 m.

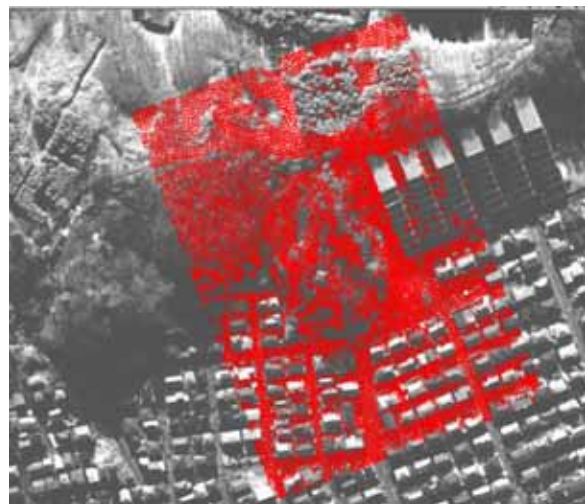


Fig. 5 Distribution of laser measurement points after filtering. Red points show measurement points

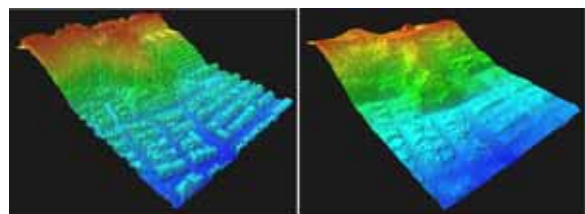


Fig. 6 Results of the filtering processing (left: before; right: after)

The interval between measurement points was 2.5 m in the track direction and 2.0 m in the cross direction. The study area was covered by 10 flight courses with a course interval of 400 m and a course overlap of 54.6 %. A 1 m

by 1 m grid was positioned over the study area and 91% of the square metres contained at least one laser measurement point.

(2) Filtering processing

In order to reveal only the ground surface, i.e. a Digital Terrain Model (DTM), it was necessary to remove the ground features from the DSM through various filtering techniques. Laser measurement points in the study area were approximated by quadratic polynomials, which gave a threshold value from 2 m to 9 m. Those measurement points over the threshold value were eliminated from the search area. Furthermore, manual processing was performed to obtain a smoother DTM. A contour map was initially drawn, on a Triangulated Irregular Network (TIN) calculated by the DTM, and the contour map was superimposed on an orthogonal colour aerial photograph. When the contour lines were dense such as on buildings or trees, on the superimposed image, laser measurement points were removed from the DTM. This manual processing was repeated several times to produce a more realistic DTM on the superimposed image (Fig. 5). The results of the filtering processing are shown in Fig. 6.

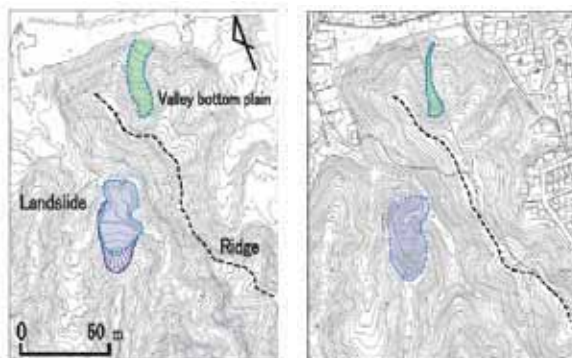


Fig. 7 (left) : 2 m grid laser contour map based on a 2 m grid DTM, and Fig. 8 (right): 1:2,500 photogrammetric map (after Tokyo City planning map, 1999).

(3) Contour map

A contour map of the study area was drawn on the DTM. First, the TIN was calculated from the DTM. At this stage, the DTM consists of randomly scattered laser measurement points. Next, 1 m, 2 m and 5 m grid DTMs were obtained from the TINs. The DTMs, here, consisted of regularly arranged points, namely grid data. Then, contour maps of 1 m, 2 m and 5 m contour intervals were drawn on the respective grid DTMs. Finally, nine kinds of contour maps (three kinds of grid intervals by three kinds of contour intervals) were produced. In terms of smooth contour lines, which express the micro topography and interpret the landforms, it was found that a 2 m interval

contour map made from the 2 m grid DTM produced the most factual results for this study area.

This contour map of the Hachioji area, called a laser contour map in this study, is shown in Fig. 7. Fig. 8 is a photogrammetric contour map. These two maps show the same place at the same scale. An aerial photographic interpretation of the micro topography of this area was also produced. It was found that the contour lines of the laser contour map, such as the ridges, valleys and landslides are very clear, and more realistic than the photogrammetric contour map.

2.2. Micro topographic details from airborne laser scanning data

As shown in Figs. 7 and 8, laser contour maps indicate micro topographic characteristics clearly and precisely. Laser contour maps are also more useful than photogrammetric contour maps to delineate landslides and other micro topographic characteristics interpreted by aerial photographs. However, laser contour maps do not always indicate actual landforms: a few errors were confirmed on valley bottoms and ridges. For example, it was difficult to filter out bamboo grasses, because the grasses are low in height (10-20 cm). However, trees were successfully filtered out, such as conifer trees, which have a height of 10-20 metres.

3. Full-scale landslide flume experiment using a rainfall simulator

Because it is very difficult to get on-site data through field observations for either case of landslide fluidization, field and model experiments have been conducted with a focus on the relationship between pore-water pressure and landslide failure process. Iverson and his colleagues (Iverson and LaHusen 1989, Iverson 1997, Iverson et al., 1997, 2000; Reid et al, 1997) performed a series of full-scale landslide experiments, and found that the pore pressure responses during sliding are significantly dependent on the initial soil porosity, and that rapid fluidized landsliding involves partial or complete liquefaction of the mass by high pore-fluid pressure. Pore pressure change induced by porosity change during landsliding depends not only on initial porosity, but also on the relative time scales for soil deformation and pore pressure diffusion. In addition, some model experiments covering “self-fluidization” have also been

performed (Eckersley 1990, Moriwaki 1993, Spence and Guymer 1997, Wang and Sassa 2003, Okura et al. 2002). In these experiments pore-water pressure generation and failure processes were examined.



Fig. 9 Model configuration before experiment.



Fig. 10 Model configuration after experiment

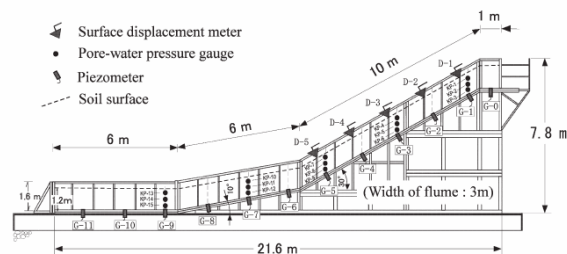


Fig.11 Model slope and location of sensors.

Although these above-mentioned results sound reasonable and interesting, some were based on small-sized flume tests. As well known, small-sized experiments have problems with scale effects, similarity relations, and the disruptive effects of sensors and their cables. Therefore, a model scale as close as possible to natural size is desirable in order to realistically reproduce a landslide phenomenon, and we performed a full-scale rainfall experiment on 16 December 2003, targeting “self-fluidization” process. We successfully initiated a landslide, and documented the slip surface formation (see Figs. 9 and 10). Data obtained on surface displacements and the

behavior of pore-water pressures before, during, and after failure were examined from a comprehensive standpoint to elucidate the fluidization process.

3.1 Full-scale model flume

The three-stage steel flume used in the landslide experiment was 23 m long, 7.8 m high, 3 m wide, and 1.6 m deep as shown in Fig.11. The main slope was a 10-m long section inclined 30 degrees, with a 6-m long section inclined 10 degrees connected at the lower end, and a 1 m long horizontal section connected at the upper end. A 6-m long horizontal extension, with the same width and depth as the sloping flume, was connected to the flume at the downslope end of the 10-degree slope. One wall of the entire flume was clear reinforced glass to enable direct observation of soil deformation. The lower end of the flume was supported by a retaining wall with a metal net for free discharge of water. Steel bars of square 1.8 cm on a side added transversely roughness to the flume’s bed at 0.12-m intervals.

The rainfall simulator in the National Research Institute for Earth Science and Disaster Prevention (NIED), Japan was used. It is 75 m long, 50 m wide, and 22 m high. This simulator is movable between five experimental sites to efficiently conduct many experiments all through the year. The simulator can sprinkle water in intensities of 15 to 200 mm/hr. The height of the nozzles above the ground was 16 m, far enough for raindrop to reach the terminal velocity. In this experiment, we sprinkled at a constant intensity of 100 mm/hr.

3.2 Monitored items

We monitored the following items with certain instruments listed below: surface displacement, piezometric level at the flume bed, pore-water pressure within the soil, slip surface locations, and landslide motion.

- 1) Surface displacement: extensometers with wire attachments were installed on the 30-degree slope.
- 2) Basal Piezometric levels: sealed diaphragm-type pressure transducers fixed to the slope bed at a regular interval of 2 m. Transducers could measure up to 3 m of pressure head.
- 3) Internal Pore-water pressures: three strain-gauge type meters were installed at regular interval of 4 m in the soil layer. These gauges were buried 30 cm, 60

cm, and 90 cm deep, respectively, at each location.

- 4) Slip surface and deformation: colored-sand indices with a width of 6 cm were inserted vertically between the soil and the glass wall at a regular interval of 1 m.
- 5) Landslide motion: high-speed video cameras and digital cameras were used. Square markers with a length of 15 cm were attached regularly on the slope surface.

Data from the sensors listed above were digitally recorded using a personal computer. Some of the sensors were monitored using a pen-recorder.

3.3 Obtained Results

The soil layer began to move after sprinkled water infiltrated to the base of the soil layer, forming a saturated zone. The soil deformation increased gradually as the groundwater level rose. Then, a rapid landslide triggered on the 30-degree slope section occurred 154 minutes 27 second (9,267 seconds) after the sprinkling started (Fig.10). Debris from this failure flowed about 4 meters downward and stopped in approximately 5 seconds. The maximum speed of the sliding mass was about 1.2 m/sec. Prior to the rapid landslide, slope deformation lasted about 41 minutes.

(1) Behavior of water pressure and surface displacement prior to the landslide

(a) Water pressure

Fig. 12 shows changes in basal piezometric levels leading up to rapid failure. All of piezometric levels increased approximately linearly with time. The piezometric level (P.L.) at G-9 where the horizontal flume was connected to the 10-degree slope (Fig. 11) responded first at about 6,300 seconds. It reached almost 110 cm of water head before the slope collapsed. Response in the horizontal layer followed later (G-11). The piezometric level at the top end (G-1) started slowly and remained the lowest until rapid failure.

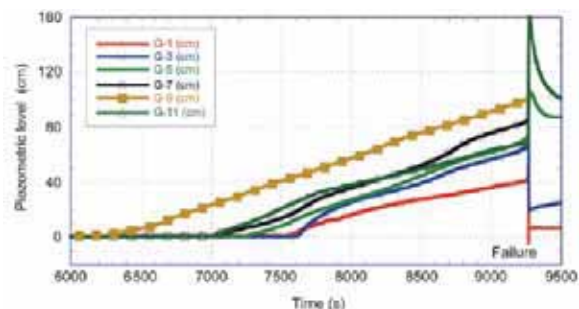


Fig.12 Change of piezometric level before the rapid slide.

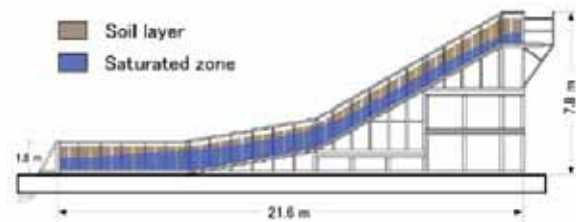


Fig.13 Inferred water table just prior to slide.

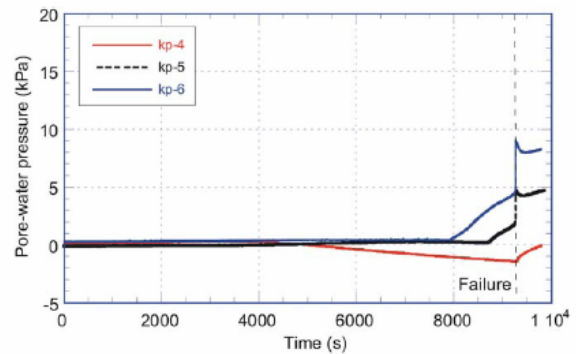


Fig.14 Change of pore-water pressure (middle part of 30 degree slope). Kp-4 is 30cm deep, kp-5 is 60cm, and kp-6 is 90cm respectively.

Fig. 13 portrays the inferred water table just prior to the rapid slide (blue-colored zone), based on piezometric levels. The highest piezometric level was recorded at G-9. The piezometric level at the horizontal part decreased gradually toward the end of the flume due to free discharge. The lowest piezometric level was recorded at the upper end of the 30-degree slope. The data indicate that the entire soil layer contained a saturated zone just before failure.

The behavior of pore-water pressure in the soil prior to slope collapse is shown in Fig.14. Pore-water pressure gauges kp-4, kp-5 and kp-6 were buried 30, 60, and 90 cm deep, respectively. Kp-6 began to rise approximately at 8,000 seconds, and kp-5 increased later. At failure both gauges reacted dramatically. The shallowest gauge of kp-4 changed to a negative state at an intermediate stage while the deepest one shifted to a positive state. As for the decreasing pore-water pressure shown by kp-4, it might be due to the possible settlement of superficial soil layer during rainfall, which would lead to a downward movement tendency for the soil layer, and then result in the increment of suction to resist this downward movement tendency. Other factors, such as temperature variation, water content, etc., may also affect the response of pore-water pressure gauge. However, because we did not measure

these items during the test, it is difficult to make a conclusive explanation here. As for the difference in the response time between kp-5 and kp-6, it may be due to the fact that the base of the soil layer was first saturated.

(b) Surface displacement

Figs. 15 and 16 show the change in cumulative surface displacement and the velocity before the rapid slide. Velocity analysis was based on data for each 30-second period. The surface displacement meter (extensometer) on the upper part of slope, D-1, began to respond at 6,780 seconds, while that on the lower part of slope, D-5, showed the most displacement until 8500 seconds, when it was surpassed by D-1 and D-3. From then on, all the sensors moved downward at an accelerating speed. The slope collapsed at 9,267 seconds when the surface displacements at D-1 and D-3 were about 4.7cm.

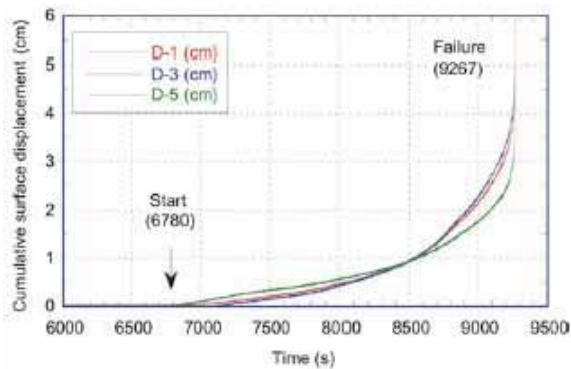


Fig.15 Change of cumulative surface displacement before the rapid slide.

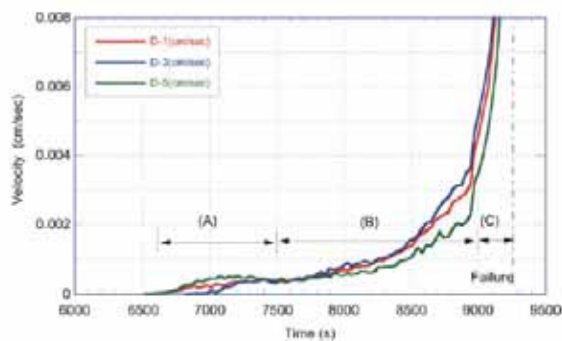


Fig.16 Change of velocity of surface displacement before slide (computed using each 30 seconds of data).

Moriwaki (2001) proposed an Index of critical strain, defined as the ratio of final cumulative displacement to the length of the source area, and four stages based on this index, a precursor stage (<0.003), a warning stage ($0.003-0.006$), a failure stage ($0.006-0.02$), and a perfect failure stage (>0.02). The critical strain in this

experiment equaled to about 0.005 (assuming that the length of the source area was 10 m), and was slightly short of the proposed failure stage values. Precursor of surface displacement lasted for 41 minutes before rapid failure. The velocity curve of surface displacement until the rapid landslide can be approximately classified into three stages; (A) asymptotic increase (about 6,500-7,700 seconds from sprinkling), (B) exponential increase (about 7,700-8,900 seconds), and (C) linear increase (about 8,900-9,276 seconds).

(2) Failure process and slip surface formation

The rapid movement during failure occurred over 5 seconds (9,267-9,272 seconds after the start of sprinkling), following the long precursory period of deformation down slope. The maximum velocity of the sliding mass was about 1.2 m/sec. The velocity of the sliding mass at failure was radically different from that before failure.

Fig. 17 illustrates the progression of the landslide for 5 seconds on the basis of deformation of white and yellow indices recorded by digital cameras. The top sketch in Fig. 17 is a side view just before the rapid slide. The bottom sketch of Fig. 17 is after the slide stopped. The other sketches are during movement. Overall, the main scarp was located at the top of the 30-degree slope and the toe was in the middle part of the horizontal layer.

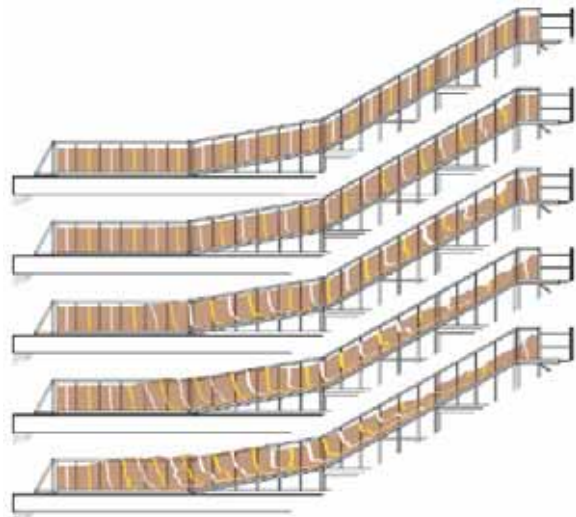


Fig.17 Illustration of soil deformation during the rapid slide. The top figure is before slide. The bottom figure is after the landslide stopped.

(3) Rapid fluctuation in piezometric levels and pore-water pressure at failure

Piezometric levels (measured by fixed sensors),

pore-water pressures (measured by unfixed sensors) rose immediately during the failure. After the rapid rise, pressures varied from place to place throughout the soil. Some pressures in the upper part of the slope declined, whereas some in the lower part of the slope gradually increased.

(a) Piezometric levels

Fig. 18 shows changes in piezometric levels (P.L.) during the rapid slide (9,267-9,272 seconds after the start). All P.L. values throughout the slope and horizontal section increased rapidly.

Small oscillations (1-2.5 Hz) in waveform were observed at sensors G-1, G-3 and G-5 in the 30-degree slope, where the soil layer slid down in parallel to the slope. The other sensors showed no remarkable cyclic fluctuations. Iverson and LaHusen (1989) reported a generation of a 1 Hz fluctuation in a 10-m long slope failure experiment. Moriwaki (1993) found in his experiment that a rapid increase of P.L. occurred during the slide. He showed the peak pressure head of the P.L. in the soil layer was approximately two times as large as the head just prior to sliding.

From the response of these piezometers and the shear displacement shown in Fig. 18, it could be concluded also that high pore-water pressures were generated during failure, i.e., were the result of failure. This supports the findings in earlier works (i.e., Iverson et al 1997, 2000; Eckersley 1990; Wang and Sassa 2003, among others). Furthermore, it is made clear that high pore-water pressure could also develop outside of the landslide mass, due to the compression induced by the landsliding mass, as shown by G-11.

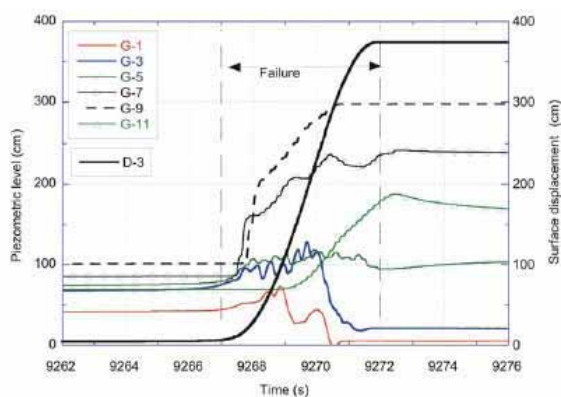


Fig.18 Fluctuation of piezometric levels during the slide (D-3; surface displacement).

(b) Pore-water pressures

As was the case with piezometric levels, all the

pore-water pressures in the soil mass rapidly increased throughout the slope as soon as rapid failure occurred. After failure pressures at some gauges decreased although most of the pressure gauges retained high-pressure states. All pressures reached the first peak within 1-3 sec after the start of sliding, and the increment in pore-water pressures was remarkable.

4. Fluidized landslide experiment on a natural slope by artificial rainfall

A rainfall-induced landslide experiment on a natural slope was conducted, which had more complex and heterogeneous characteristics than the indoor models, in an attempt to investigate the dynamic movements of the soil surface, the formation of the sliding surface, and hydrological characteristics, based on the results of the indoor flume testing. Landslide experiments on natural slopes by sprinkling or water supplying from trenches have been reported four times in Japan and U.S.A. The respective conditions for each experiment are shown in Table 1.

The experimental slope was 30 m long and 5 m wide, and mainly covered by weathered disintegrated granite sand. Soil-surface movements were monitored by using stereo photogrammetry (5 stereo pairs of CCD video cameras). Hence white-coloured targets were placed on the experimental slopes and the movements of these targets were traced by image analysis. To detect the formation of the sliding surface, soil-strain probes were inserted into the soil to 2 m depth at deepest. Tensiometers were used to measure changes in pore-water pressures within the soil.



Fig. 19 View of the experiment site at Mt. Kaba-san.

The purpose of this experiment is to produce hopefully a fluidized landslide on a natural slope by

artificial rain fall. The test site was selected by two conditions; 1) to secure complete safety during the experiment, 2) to have a possibility producing a fluidized landslide. Then, a natural slope in the Koido National Forest at Mt. Kaba-san, Yamato village, 25 km north of Tsukuba-city, Ibaraki Prefecture, Japan was selected for the controlled experiment on landslide and possible fluidization in cooperation with the Forestry Agency of Japan.

The selected portion of hillslope (Fig. 19) was 30 metres long, with an average gradient of 33 degrees (maximum 35 degrees). The soil was 1 to 3 metres deep. A 5-m-wide experimental slope was isolated from its surroundings by driving thin steel plates about 1-m-deep into the soil. These plates prevented lateral diffusion of infiltrated rain water and cut the lateral tree root network that imparts resistance within the soil layer. The surface of the slope was covered by straw matting to prevent surface erosion and promote rainfall infiltration. Surface material on the slope consisted of fine weathered disintegrated granite sand, called “Masa” in Japan. Loamy soil blanketed the upper portion of the regolith to a depth of about 1 m; this soil mainly originated from tephra of Mt. Fuji, Mt. Akagi, and other volcanoes located west of Mt. Kaba-san.

Artificial rain at the rate of 78 mm/h was applied to the slope segment during the experiment by way of a rainfall simulator. The simulator consisted of a framework of steel pipes with 24 sprinkling nozzles arranged 2 m above the soil surface. Water for sprinkling was pumped from a dam constructed in a small creek at the base of the slope into 80 water storage tanks (1 m³ for each) on the neighboring hillslope prior to the experiment.

To obtain information on the formation of the sliding surface, four soil-strain probes were inserted. The diameter of the probes was only 10mm and they

were specially prepared. To measure saturation conditions within the soil, tensiometers with porous ceramic cups were set into the slope.



Fig. 20 Views of the debris flow resulting from the landslide fluidization between five seconds and seven seconds after failure.

4.1 Overview of the triggered landslide movement

On 12 November 2003, artificial rainfall was given to the slope at a rainfall intensity of 78 mm/h for four hours and a half until sunset. No slope movement was observed. The second experiment was conducted on 14 November 2003. Artificial rainfall started from 9:13 at a rainfall intensity of 78 mm/h, the slope deformation was detected from around 15:00, then a clear movement was observed beginning at 16:03. The

Table 1 Examples of landslide experiments in natural slopes.

References	Location	Volume W × L	Excavation etc.	Water supply	Sensors	Fluidization
Oka 1972	Ikuta, Kawasaki, Japan	500 m ³		Sprayed from fire hose		Yes
Yagi, Yatabe, & Enoki, 1985	Matsuyama, Japan	10 × 25 m	Trench cut at upper and both sides	Rainfall simulator (Sprayed on upper half slope)	Extensometer Piezometer Strain meter	Yes
Yamaguchi, Nishio, Kawabe, Shibano, & Iida, 1989	Yui, Shizuoka, Japan	10 × 30 m	Upper trench cut Lower open cut	Supplied from upper trench	Extensometer Piezometer Inclinometer	No
Harp, Wells & Samiento, 1990	Utah, USA	1.6 × 1.3 m 2.0 × 2.2 m 3.2 × 4.0 m	Upper trench cut Lower open cut	Supplied from upper trench	Extensometer Piezometer	No

initiated landslide was a type of an expected fluidized landslide, the landslide mass rapidly moved and travelled long.

The cover of the tensiometer started to incline downslope at 24,627.5 sec (410m 27.5s) after sprinkling commenced. We interpret this as indicating that slope failure initiated at 24,627.5 sec.



Fig. 21 The landslide deposit one day after the experiment.

Images at 24,632.5 sec (5 sec after failure) and 24,634.5 sec (7 sec after failure) are shown in Figs. 20a and b. Fig. 20 presents the movement of liquefied landslide mass. The failed landslide mass had entered the stream and was about to collide with the confronting slope (Fig. 20a). After collision, the fluidized landslide turned to the right (Fig. 20b), changed into a debris flow, and travelled downstream for 10 seconds on about 10 degree gradient, as much as 30 m. It took 17 seconds from the initiation of the landslide to the end of deposition. Fig. 21 shows the landslide deposit one day after the experiment. The straw matting, the cover of the tensiometers, and the white-coloured targets were conveyed to the toe of the fluidized landslide.

4.2 Observation of sliding-surface formation process

When a sliding surface forms, soil above the sliding surface tends to move downslope, whereas soil below it remains stable. Fig. 22 shows the accumulation of soil strain during the experiment. The results from soil-strain probe P3 is shown in Fig 22a, and for P4 in

Fig. 22b. For the strain probe at P4 (Fig. 22b), positive values of strain were observed at a depth of 70 cm from about 20 minutes after sprinkling began, and negative strains at a depth of 60 cm. We interpret from the paired positive and negative values that the sliding surface formed between 60 cm and 70 cm depth. At failure (410 minutes), the accumulated strain at a depth of 70-cm was larger than 0.04, which was the capacity of the strain gauge. Similar results were obtained at P3 (Fig. 22a). Positive values of strain were observed at 120 cm depth from about 300 minutes and negative values at 110 cm depth, indicating a sliding surface between 110 cm and 120 cm depth. The depth of sliding at P3 was twice as deep as at P4.

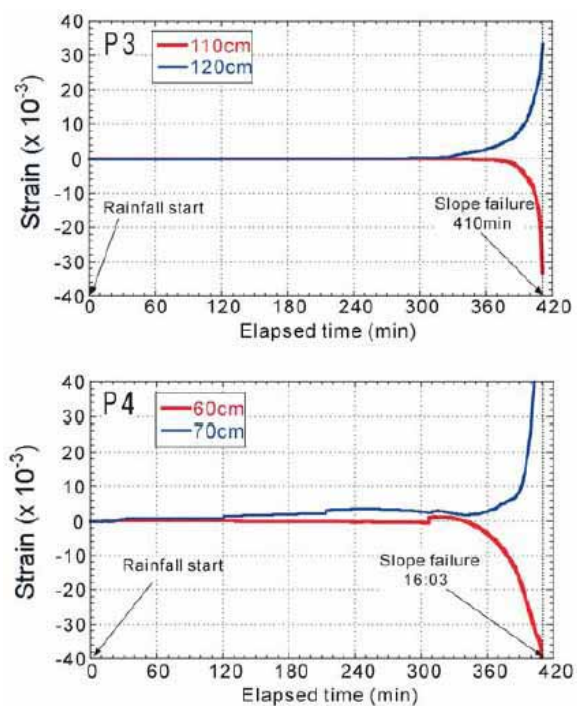


Fig. 22 Soil-strain accumulation curves. (a) at P3 and (b) at P4.

Changes in pore water pressure including suction monitored by the tensionmeters are presented in Fig. 23. The tensionmeters were placed at depths of 50, 100, 150, 200, 250, and 290 cm. All tensionmeters showed negative pore pressures at the start of sprinkling, indicating that the soils at all depths were unsaturated or partly saturated. When the wetting front passed, the tensionmeters showed increases in pore pressure in sequence of the depths. At 410 min, when the failure took place, all of the tensionmeters showed positive pore pressures. The pore pressure of the deepest tensionmeter (290 cm) rapidly increased its values from about 290

min. This almost coincided with the time when the strain gauge at 110 cm depth in the strain probe at P3 started to show strain (Fig. 22a). Hence, it can be deduced that general slope instability increased from 290 min, before final failure at 410 min.

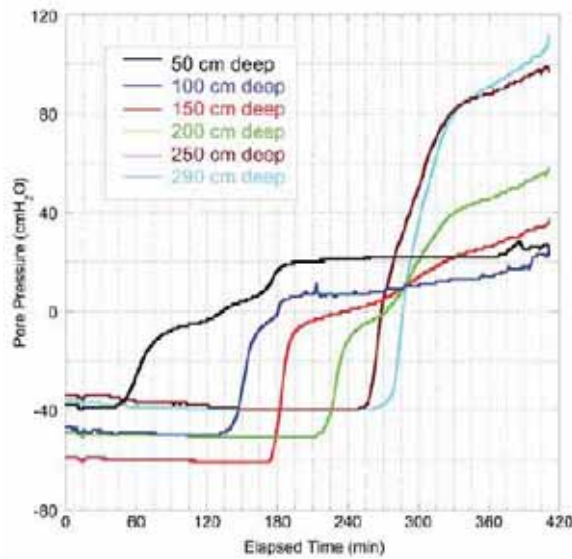


Fig. 23 Changes in soil-water pressure in tensiometers.



Fig. 24 Air photo of the densely populated developed area near Tokyo (A: Hino site; B: Hachioji site).

5. Landslide risk evaluation and hazard zoning for rapid and long-travel landslides in urban development areas

The APERITIF project comprises landslide risk evaluation and urban hazard zoning for rapid and long-travel landslides, conducted in two selected sites in Japan. One is the upper slope connecting to the site

of 1995 Nikawa landslide (34 fatalities, Fig. 24) triggered by the Hyogoken-Nambu earthquake in Nishinomiya city between Osaka and Kobe; the other site corresponds to slopes inside or adjacent to a large scale residential development in the Tama hills near Tokyo. Locations of the investigated sites are shown in Fig.25. Achievements in the study on 1995 Nikawa landslide site was reported in Sassa et al. (2004). In this section, recent achievement of the assessment of rapid and long-travel landslides which will be triggered by future huge earthquake in a densely populated residential town near Tokyo.



Fig. 25 Location map of study areas



Fig. 26 Air photo of the densely populated developed area near Tokyo (A: Hino site; B: Hachioji site).

5.1 Field study for the development area near Tokyo

During the 1923 Kanto earthquake, 142,800 persons were killed. There have been no other large earthquakes since. However, it is not possible to predict how long this situation will continue. The return period of big earthquakes in the Tokyo area is estimated to be about 69 years (Kawasumi 1970). Large-scale urban development after 1923 in and near Tokyo has been extensive. To assess landslide vulnerability of sandy slopes that are widespread in the Tama hills (a residential area of Tokyo), a large-scale experiment was conducted in November 1971 as a joint project of

the research institutes of several ministries of the Government of Japan. In this in-situ experiment, six boreholes were conducted, 10 extensometers and other instruments were installed on the field, where the preparatory artificial rainfall events were repeated since May 1971, and finally a landslide was triggered (Oka, 1972). However, the landslide that was triggered was far more severe than had been anticipated, since it was much faster and travelled much further than had been allowed for. 15 people, including technical observers and journalists, were killed and more than ten persons were injured. At that time, rapid and long-travel landslides could neither be understood nor predicted. They are still top targets of landslide research; they are the research rationale of APERITIF. In another view, this event demonstrated the risk of rapid and long-travel landslides in this area by a real event.

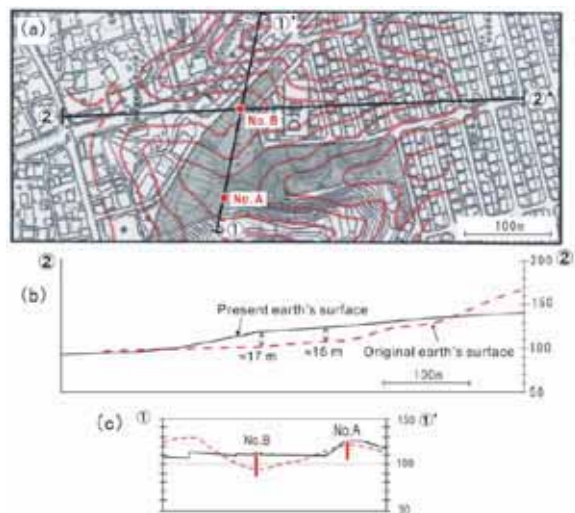


Fig. 27 Topographic map of the infilled valley and locations of sections in the Hino area. Red contours show ground levels in 1940 prior to infilling. (a) Topographic map, (b) Longitudinal section of 2-2', (c) Cross section of 1-1'

(1) General description of the area

Fig. 26 shows a study area in the hilly Tama area near Tokyo. It is located at the border of Hino and Hachioji cities. The area is covered by an almost flat sedimentary sandy layer (Kazusa group soil), which was formed during the Pliocene and Pleistocene. Two sites, A and B, were selected in this area. Site A is a large infilled valley within the residential area. Site B is an projecting ridge toward the residential area. Those areas are shown in the rectangular boxes in Fig.26. Fig.27a shows a topographical map including the red

colour contour lines of the 1940 map for part of infilled valley. Fig.27b presents its longitudinal section, and Fig.27c shows its cross section. Those two sections indicate that a valley 15-17 m deep was filled over 300m to develop the flat residential area. Fig. 28 shows the topography and geological sections of site B. Fig.29 presents photos of the Site B in the Hachioji city.

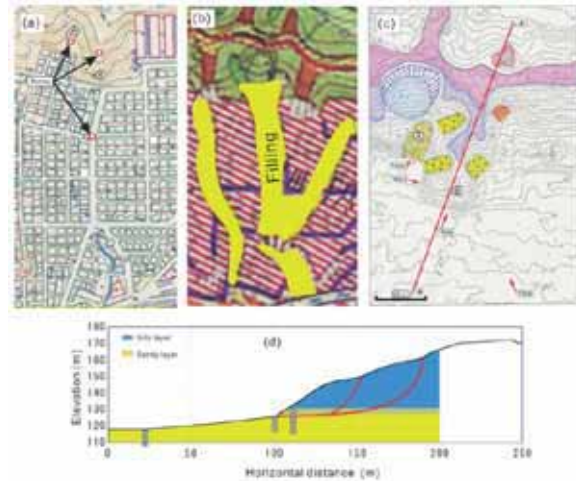


Fig. 28 Map of the Hachioji site. (a) Present topographic map, (b) location of the infilled valley, (c) Topographic ground surface map obtained by removing the effects of forests and houses by the laser scanner technology, and (d) geological cross section along A-A in (c).



Fig.29 (a): a general view of the developed residential area. The red arrow indicates the location of the extrusive ridge, (b): front view of the ridge, (c): side view of the ridge, (d) : ground water indicating that a saturated zone exists below the ridge because bedding planes in the area are almost flat.

Sedimentary sandy layers are distributed through almost horizontal bedding, so this saturated sandy layer should extend below the extrusive ridge. To investigate this situation, four drillings were planned. However, due to non-cooperation of a development company in this area, two drillings could not be conducted along the central section. So they were drilled some distance

apart at a higher elevation. As a result, the geological section presented in Fig. 28d was obtained. The blue colour part indicates an unsaturated silty layer. Probably this layer cannot experience rapid and long-travel landslides. However, if the saturated sandy layer will be liquefied or semi-liquefied during earthquake loading, there is a high possibility of landslides along the sliding surfaces because most resisting parts in these expected landslides are parts passing inside the saturated sandy layer.

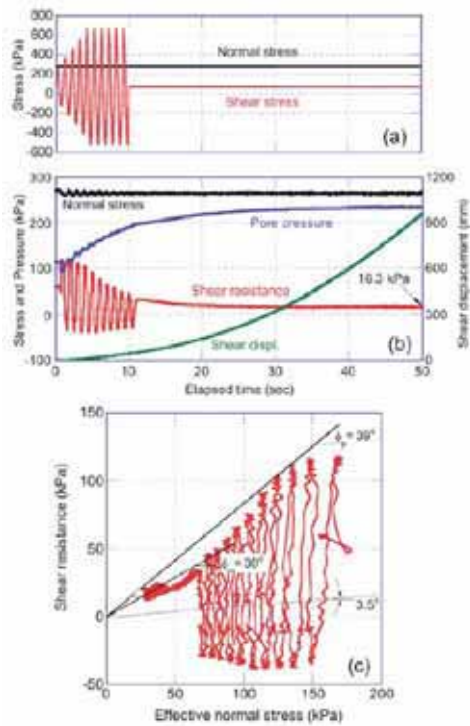


Fig. 30 Undrained cyclic loading test on a sample taken in the Hino area ($B_D = 0.96$). (a) Control signal for normal stress and shear stress, (b) Time series data, (c) Stress path. Note that values of 39 and 30 degrees in Fig. 30c were approximate estimated in reference to Fig.32 and Fig.33 because pore pressure was not accurately measured except the value in the steady state.

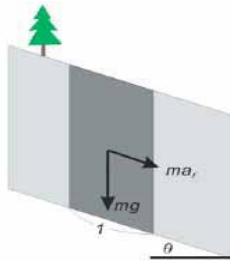


Fig. 31 Shear stress increment due to seismic acceleration. Here, $\Delta \tau_f = ma_f$

(2) Experiments for landslide risk evaluation during earthquakes

Two boreholes (A and B) were drilled at the Hino site (Fig 27). Samples were taken from the filled materials in the infilled valley. An undrained cyclic shear stress loading test was performed to assess the acceleration required to cause failure. An initial normal stress conditions to reproduce the potential sliding surface of 15 m deep in a 12-13 degrees slope were applied. The initial ground water table was 2.5 m from the surface. Therefore, an initial pore-water pressure of about 120 kPa (corresponding to the water table above the sliding surface) was imposed. A control signal to produce the required cyclic shear stress by increasing its value step by step up to around 600 kPa ensured the occurrence of failure. As seen in Figs.30b, c, the mobilized maximum shear stress was about 115 kPa (which corresponds to 220 gal) in shear stress increment to cause failure from the following relation (see Fig. 31).

$$a_f = (\Delta \tau_f / m) = (\Delta \tau_f / \tau_0) \times g \sin \theta \quad (1)$$

Here, m : mass of a unit column between the ground surface and the potential sliding surface, θ : angle of the potential sliding surface, τ_0 : Initial shear stress due to self weight of the column acting on the sliding surface, $\Delta \tau_f$: seismic shear stress increment required to cause failure ($= ma_f$), a_f : seismic acceleration to cause the above seismic shear stress

The steady state shear resistance reached 16.3 kPa. The apparent friction angle was only 3.5 degrees. It is a typical sliding surface liquefaction. Rapid and long-travel landslides should result from such stress condition.

Then, a naturally drained cyclic loading test using the same sample, control signal testing procedure with the undrained test (Fig.30) was performed. The test results are shown in Figs.32a, b. These are similar to the undrained test, although the excess pore pressure could not be monitored because the pore pressure transducer inlet is located 2 mm above the shear surface. Excess pore pressure was generated within the shear zone (there, grains are crushed and causing a decrease in permeability). The influence of open valve drainage is much great. However, the shear resistance decreased until 29kPa and shear displacement accelerated. It is apparently the sliding surface

liquefaction phenomena. The steady state shear resistance was around 1.8 times greater than in the undrained test. The difference can be explained by pore pressure dissipation. The real soil response should fall in between these extremes.

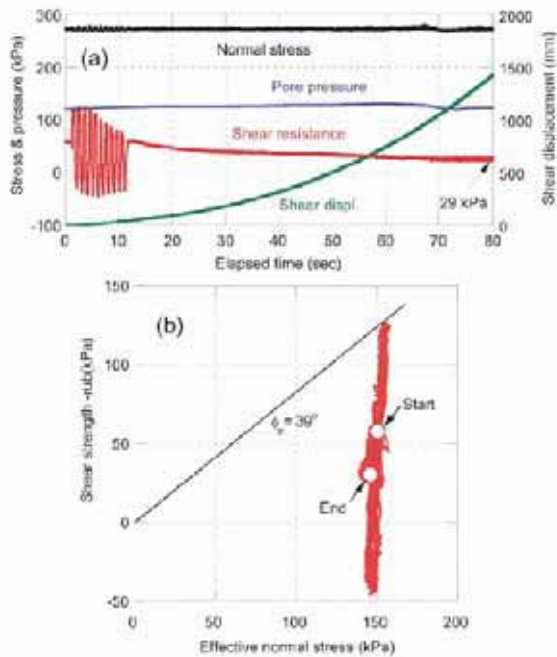


Fig. 32 Naturally drained cyclic loading test on a sample taken in the Hino area ($B_D = 0.97$). (a) Time series data, (b) Stress path.

Fig. 33 presents the result of a test on a sample taken from sands in the Hachioji area. The control signal for cyclic loading is the same as in previous case. However, the initial condition is different. Initial normal stress and shear stress corresponding to a depth of 20 m in a 10 degrees slope without initial pore water pressure were reproduced. The slope is in the projecting ridge, therefore a high ground water level is not expected in ordinary period without rainfall, while the bottom of ridge (sandy layer) is expected to be saturated. In the simulating experiment failure took place for a shear stress around 151 kPa, corresponding to a critical seismic acceleration of 270 gal. The steady state shear resistance was 35 kPa, and the apparent friction angle was 4.5 degrees. This value is low enough to suggest the possibility that long-travel landslides will be a potential hazard in this area.

If a landslide fails from the slope onto the residential area, then the loading is undrained. The ground water table is shallow (as suggested by photo of Fig.29d) and the infilled valley in front of this part of slope shown in

Fig.28b provides a further problem. The case of undrained loading was analyzed and illustrated by Sassa et al. (1997) and by Sassa et al. (2004) which is introduced in Fig.34. The landslide mass causes a static stress increment due to the increase of self weight (ΔW) and provides a dynamic stress increment F_d when it is moving. It is expressed by using the dynamic coefficient (k_d)

$$F_d = k_d \times \Delta W$$

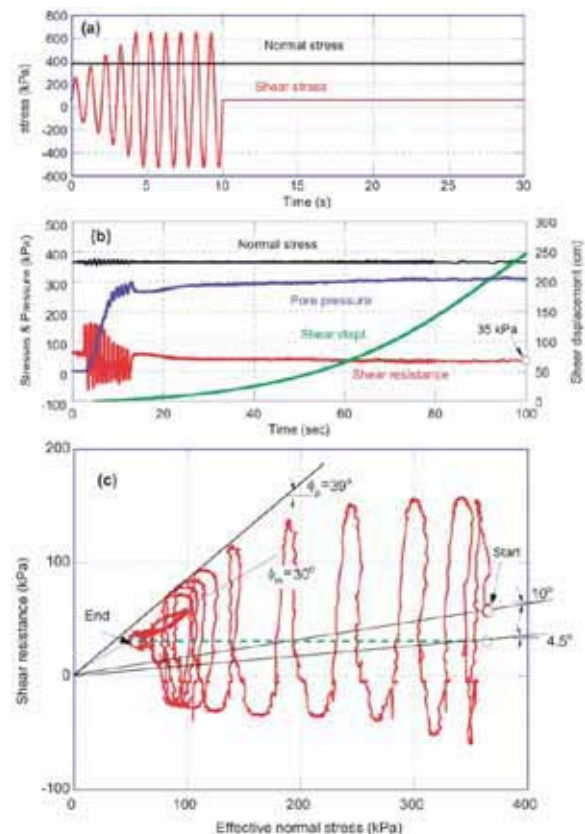


Fig. 33 Undrained cyclic loading test of the sample using the drilling core in the Hachioji area ($B_D = 0.99$). (a) Control signal for normal stress and shear stress, (b) Time series data, (c) Stress path.

Using the same sample as in previous tests, an undrained dynamic loading test was conducted. The normal stress was 380 kPa, corresponding to a depth of 20 m, and the initial normal stress corresponding the depth of infilled valley (or the depth of the saturated layer) corresponds to around 2 m deep. A dynamic coefficient of 0.9 was assumed. The test results presented in Fig. 35 shows that the mobilized steady state shear resistance was 5 kPa. Based on those values, a computer simulation based on the geotechnical approach (Sassa, 1988) was conducted to predict the

hazard area.

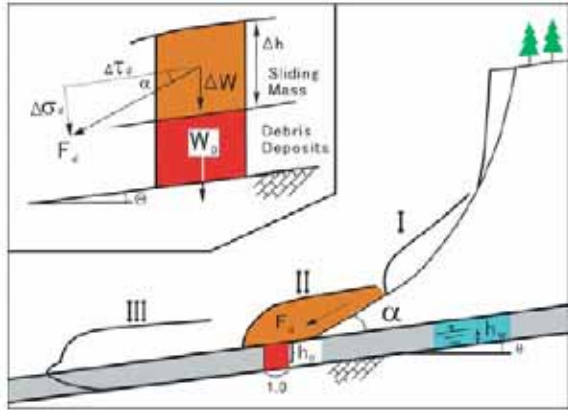


Fig. 34 Model of the landslide triggered debris flow (Sassa et al. 1997).

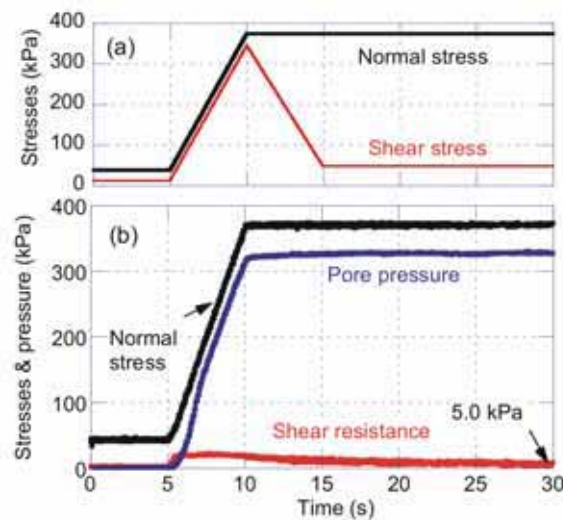


Fig. 35 Test to simulate the undrained loading on the filling in valley in the Hachioji area. (a) Control signal, (b) Time series data of normal stress, shear resistance, and pore-water pressure.

5.2 Computer Simulation in investigated areas

A geotechnical landslide simulation model was proposed by Sassa 1988. It was improved to a computer code for general use during APERITIF project especially in the data input and three dimensional presentation of output. This new computer code for rapid landslides (Rapid/LS) was applied to reproduce the two cases using the measured values of the steady state shear resistance obtained through undrained and naturally drained ring shear tests. In addition to the steady state shear resistance, another parameter for geotechnical simulation, the lateral pressure ratio $K (= \sigma_h / \sigma_v)$ was introduced to express

“softness” or “potential for lateral spreading” of the moving mass. According to the parameter, the lateral pressure acting on a soil column is close to 1.0 if the material appears to be liquid. Liquid spreads laterally without limitation on the flat plane. In contrast, if the material is completely rigid (like metal or a rock mass), the lateral pressure ratio $K = 0$. A hard rock can stand on the plane and never spread laterally. Soils are in between. It will be reasonable to assume that the value inside a moving soil mass will be between 0 and 1, though the lateral pressure ratio in the static soil mass can be more than 1.0 under the over consolidated state.

The value was expressed using the mobilized apparent friction angle inside the soil mass (ϕ_{ia}) as an extension of Jaky’s equation of the lateral pressure ratio at rest in the first time loading (Lamb & Whitman 1979) to the lateral pressure within a moving soil mass (Sassa, 1988).

$$K = 1 - \sin \phi_{ia}$$

the mobilized apparent friction angle inside the soil mass (ϕ_{ia}) is estimated

$$\text{where } \tan \phi_{ia} = \{c + (\sigma - u) \tan \phi_i\} / \sigma$$

$\tan \phi_{ia}$ is the mobilized friction angle during the moving soil mass which must be between the peak friction angle and the friction angle mobilized during motion. Usually the value will be the friction angle mobilized during motion (ϕ_m), namely the effective friction angle obtained in the ring shear test reproducing landslide motion or those in Sassa et al. (2004) and cohesion will be zero. However, if the soil mass moves with an undisturbed state except the sliding surface like the Takarazuka landslide, Japan during the Kobe earthquake in 1995 (Sassa 1996, Sassa 2000), the $\tan \phi_i$ can be between ϕ_p and ϕ_m , and cohesion is not always zero. Therefore, ϕ_{ia} take a greater value, then K can be smaller.

This value was assumed higher for the Hino site (0.65 – 0.80) because the ground water table was high and the landslide mass was almost saturated based on approximate estimation; $\phi_i = 30$ degrees, $c = 0$, $(\sigma - u) / \sigma = 0.58$ (15 m in depth of soils and 12.5 m in water depth above the sliding surface) leads to the calculation of ϕ_{ia} as 18.5 degree. Then, it gives the value for $K = 0.68$. The value will be getting greater when mobilization during motion will increase pore water pressure. Then, it was assumed to be in the range

of 0.65-0.80 in this simulation.

Similar consideration was made for the Hachioji site, then, it was assumed relatively lower (0.50 – 0.65) because the landslide mass was normally less saturated. For both cases, a higher K value was given in the lower parts of travel area because the landslide mass should be more mixed and lose its original structure, namely should become soft.

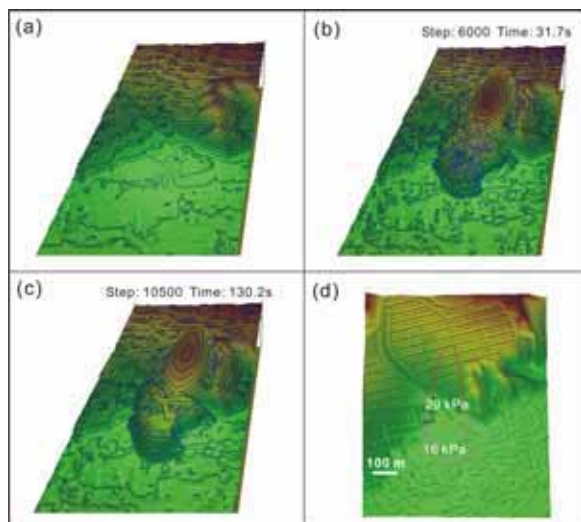


Fig. 36 Results of simulation results for Hino area (shear strength at steady state: 16 kPa). (a) original topography, (b) and (c) during motion, (d) deposited areas corresponding to the steady-state-shear strength of 16 and 29 kPa, respectively. Lateral pressure ratio $k=0.65-0.80$. The three dimensional view was made by the Geographical Survey Institute of Japan.

The first case concerns the Hino residential site, a part of which was constructed in the infilled valley. Fig. 36 presents three-dimensional visual output of the result; Fig. 36a shows the initial state, Fig. 36b shows an intermediate stage during motion; Fig. 36c reports the final deposition state; and Fig. 36d presents the assessed hazard area superimposed to the three dimensional view of the area obtained by the laser scanner technology (Japanese Geographical Survey Institute). In the Fig. 36d, the larger area corresponds to the data obtained by the undrained ring shear test (using 16 kPa as the steady state shear resistance), and the smaller area corresponds to the naturally drained ring shear test (using 29 kPa as the steady state shear resistance). The scale of the landslide is rather large for landslides in urban areas, because the head of the landslide in the source area and the toe of landslide after deposition will be 480 m (under the undrained

condition). The hazard area is much greater in this case. However, since the source area includes many houses, the assessed risk is quite large even for the naturally drained case.

The second case concerns the Hachioji site, which is at risk due to a landslide located in an adjacent steep slope. As parameters 35 kPa for the steady state shear resistance is expected and 5 kPa in the undrained loading area. The rapid loading test under naturally drained condition has not yet been conducted. The value must be higher. Using the ratio of steady state shear resistances between undrained state and naturally drained case on the Hino area ($29/16=1.8$), the value can be around 10 kPa.

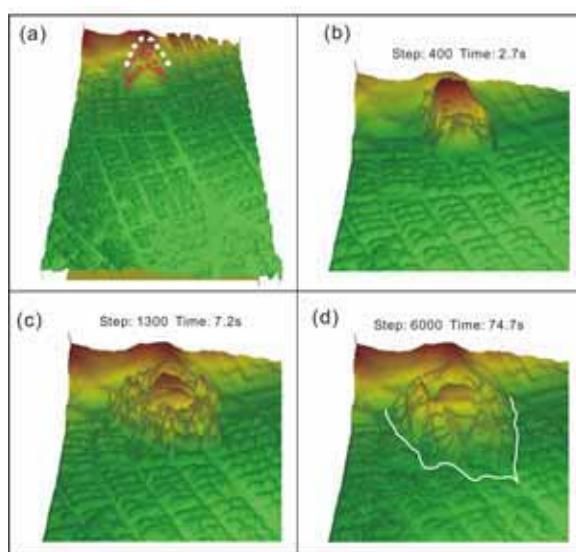


Fig. 37 Simulation results for Hachioji area (shear strength at steady state: 16 kPa). (a) original topography, (b) and (c) during motion, (d) deposited area. (Three-dimensional view was made by the Geographical Survey Institute of Japan using the laser scanner data for this APERITIF project. Lateral pressure ratio $k=0.50-0.65$.)

Further works are necessary to obtain a reliable hazard zoning for this site, however, a computer simulation was applied using those values of parameters and the detailed topography obtained by the airborne laser scanner as a reference.

Fig. 37 shows the results for the case of 20 m deep landslide mass onto the infilled valley in the Hachioji area; Fig. 37a presents the initial state before landslide in which some steps as possible head scarps are visible; Fig. 37b and Fig. 37c show an intermediate state during motion; Fig. 37d is the final situation after deposition in

which the border of deposited landslide mass is delineated. The landslide mass covered a considerably large area along the infilled valley.

6. Conclusion

The following conclusions can be drawn:

- (1) Airborne laser scanning was carried out in the Tama Hills to produce laser contour maps. It was found that laser contour maps depicted landforms, such as the break in slopes and landslides, more precisely than photogrammetric contour maps.
- (2) A full-scale landslide experiment was conducted to clarify the failure process of a landslide triggered by rainfall, using a loose sandy soil. A complete shear zone (sliding surface) was formed within the soil layer, and the displaced soil mass on the upper slope section moved as a unit, while the lower parts were compressed. When a slope consists of loose soil with high water content, the pore-water pressures can increase remarkably during failure and simultaneously decrease the shear strength of the slope. In this experiment, a large saturation zone and a rapid increase of subsurface water pressures throughout the soil layer during failure were observed.
- (3) An experiment to induce a fluidized landslide by artificial rainfall was conducted on a natural slope. It first slid, then fluidized, and changed into a debris flow. Formation of the sliding surface was detected by soil-strain probes. The tensiometer showed a rapid increase in pore-water pressure after about 290 min from the start of sprinkling. This almost coincided with the time when the strain was first observed on the sliding surface.
- (4) Landslide risk evaluation for rapid and long-travel landslides triggered by earthquakes was conducted using data obtained by the ring shear tests on samples from drilling cores, together with geological and topographical investigation of the sites. The results of investigation for three selected sites in the Nikawa area and the Tama area near Tokyo presented above show that all three sites could be subject to sliding surface liquefaction with resulting rapid and long travel earthquake induced landslides.
- (5) Ring shear tests to reproduce stresses and shear displacement during and after earthquakes were

conducted in undrained conditions and in naturally drained conditions by opening the drainage valve on the top of ring shear box. Results from the naturally drained test for the silty gravel layer of the Nikawa landslide and the sandy fill material of the Hino site are consistent with sliding surface liquefaction and rapid post-failure motion. However, the naturally drained test for the sandy layer of the Nikawa landslide did not produce parameters consistent with sliding surface liquefaction, and the shear displacement which started during the main shock terminated at less than 7cm, probably because the pore pressure dissipation rate from the shear zone is great enough comparing with pore pressure generation rate in the shear zone. This suggests that the landslide risk is affected by both of pore pressure generation in the shear zone and pore pressure dissipation from the shear zone. The drainage path in the ring shear test is shorter than the real state, therefore, the real state in the slope will be between both of the undrained state and the naturally drained case.

- (6) The geotechnical computer simulation code (Rapid/LS) using geotechnical data obtained by the ring shear tests and detailed topographical data obtained by laser scanner presented urban hazard zoning for rapid landslides in two densely populated residential sites near Tokyo. The parameters will be different for the expected landslide movement mode depending on whether the sliding surface will be formed inside the landslide mass or inside the ground layer over which the landslide mass moves. For the Hachioji site, the test data obtained from the ring shear test to simulate the undrained loading of landslide mass onto the infilled valley by assuming that the sliding surface will be formed inside the ground was used in the traveling area. Reliable hazard zoning needs careful examination for the expected landslide movement mode. However, the method proposed here seems a reliable and convincing approach of urban hazard zoning based on the geotechnical parameters at street-level scale for these two sites.

Acknowledgments

This research was conducted as a part of the Areal Prediction of Earthquake and Rain Induced Rapid and Long-Traveling Flow Phenomena (APERITIF) project of the International Programme on Landslides (IPL M101), which was funded by the Special Coordinating Fund for Promoting Science and Technology of the Ministry of Education, Culture, Sports, Science and Technology (MEXT) in 2001-2004.

This APERITIF project was also supported by all group members of this project including members of University of Tokyo (Ikuo Towhata, Kazuo Konagai), the Japan Landslide Society (Takahiko Furuya, Chigira Masahiro), Niigata University (Hideaki Marui), and this research was benefited from the advice of Prof. Osamu Sato, Prof. Akira, Iwamatsu and Dr. Norio Oyagi of the project management committee.

The authors deeply appreciate the cooperation of the office of Disaster Prevention Research of MEXT for its cooperation with the implementation of this project. The authors also appreciate the members of Research Centre on Landslides of Disaster Prevention Research Institute of Kyoto University for their cooperation.

References

- Ackermann, F. (1999): Airborne laser scanning present status and future expectations. *ISPRS Journal of Photogrammetry and Remote Sensing*, 54: 64-67.
- Aleotti, P., Canuti, P., Iotti, A., and Polloni G. (2000): Debris flow hazard and risk assessment using a new airborne laser terrain mapping technique (ALTM). *Proceedings of the International Symposium on Landslides, Cardiff, June 2000*, 1, pp. 19-26.
- Ambraseys, N.N. and Bommer, J.J. (1991): The attenuation of ground accelerations in Europe. *Earthquake Engineering & Structural Dynamics*, 20:1179-1202.
- Bishop, A.W. (1973): The stability of tips and spoil heaps. *Quarterly Journal of Engineering Geology*, 6: 335-376.
- Bromhead, E.N. (1979): A simple ring shear apparatus. *Ground Engineering*, 12(5): 40-44.
- Eckersley, J.D. (1985): Flowslides in stockpiled coal. *Engineering Geology*, 22: 13-22.
- Eckersley, J.D. (1990): Instrumented laboratory flowslides. *Geotechnique* 40(3):489-502.
- Fukuoka, H., G. Wang, K. Sassa, F. Wang and T. Matsumoto (2004): Earthquake-induced rapid long-traveling flow phenomenon: May 2003 Tsukidate landslide in Japan. *Landslides*, Vol. 1, No. 2, Pages: 151 - 155.
- Fukushima, Y. and Tanaka, T. (1990): A new attenuation relation for peak horizontal acceleration of strong earthquake ground motion in Japan. *Bulletin of the Seismological Society of America*, 80 (4):757-783.
- Fukuzono, T. (1985): A new method for predicting the failure time of a lope. *Proceedings of IVth International Conference and Field Workshop on Landslides, Tokyo, 23 - 31 August, 1*, 145 - 150.
- Geographical Survey Institute, Japan (1996): Active fault map in urban area: Northwest part of Osaka.
- Hanshin Water Supply Authority and Nippon Koei Co. (2002): Analysis of the landslide risk due to the construction of the Kozhan regulating pondage (report, in Japanese), 200p.
- Harp, E.L., Wells, W.G. and Sarmiento, J.G. (1990): Pore pressure response during failure in soils. *Geological Society of America Bulletin*, 102, 428-438.
- Hasegawa, H., Okamatsu, K. (2001): Detailed landform feature and characteristics extraction with high dense DTM data. *Proceedings of the autumn conference of the Japan Society of Photogrammetry and Remote Sensing, JSPRS*, pp. 189-192 (in Japanese).
- Hatori, K. and Juen, S. (1958): The Quaternary history of the western margin of Kanto basin (I), (II). *The Journal of the Geological Society of Japan*, 64: 181-194, 232-349 (in Japanese with English abstract).
- Hutchinson, J.N. (1986): A sliding-consolidation model for flow slides. *Canadian Geotechnical Journal*, 23: 115-126.
- Irikura, K. (1996): Strong ground motion of the Hyogoken-Nanbu earthquake and the fault model (in Japanese). *The Great Hanshin-Awaji Earthquake Disaster for the Disaster Prevention Research, DPRI, Kyoto University*, pp 81-98.
- Ishihara, K. (1993): Liquefaction and flow failure during earthquakes. *Geotechnique*, 43(3): 39-46.
- Ishihara, K., Okusa, S., Oyagi, N. and Ischuk, A. (1990): Liquefaction-induced flowslide in the collapsible loess deposit in Soviet Tajik. *Soils and Foundations*, 30(4): 73-89.
- Iverson, R.M., Reid, M.E. and LaHusen, R.G. (1997): Debris-flow mobilization from landslides. *Annual Review of Earth Planetary Science* 25:85-138.
- Iverson, R.M. (1997): The physics of debris flows.

- Reviews of Geophysics 35(3): 245-296.
- Iverson, R.M. and LaHusen, R.G. (1989): Dynamic pore-pressure fluctuations in rapidly shearing granular materials. *Science*, 246: 769-799.
- Iverson, R.M. and LaHusen, R.G. (1989): Dynamic pore-pressure fluctuations in rapidly shearing granular materials. *Science* 246:796-799.
- Iverson, R.M., Reid, M.E., Iverson, N.R., LaHusen, R.G., Logan, M., Mann, J.E. and Brien, D.L. (2000): Acute sensitivity of landslide rates to initial soil porosity. *Science* 290:513-516.
- Kaizuka, S., Koike, K., Endo, K., Yamazaki, H., Suzuki, T. (2000): Landforms, no.4, Kanto and Izu Ogasawara. 349pp, University of Tokyo press. (in Japanese).
- Kamai, T. et al. (1995): Landslides in the Hanshin urban region caused by the 1995 Hyogoken-Nanbu earthquake, Japan (in Japanese). Investigation Report of landslides induced by the Hyogoken-Nanbu Earthquake and others, The Japan Landslide Society, pp 33-58.
- Kawasumi, H. (1970): Verification of 69-year Periodicity of the Kanto Nanbu Earthquake and the Imminence of its Occurrence and the Emergency in Countermeasures and Problematic Points. *Chigaku Zasshi* (in Japanese), 79(3):115-138.
- Konagai, K., Johansson, J., Mayorca, P., Yamamoto, T., Miyajima, M., Uzuoka, R., Pulido, N., Duran, F.C., Sassa, K. and Fukuoka, H. (2002): Las Colinas landslide caused by the January 13, 2001 off the coast of El Salvador earthquake. *Journal of Japan Association for Earthquake Engineering*, 2(1):1-15.
- Lambe, W. and Whitman, R. (1979): General aspects of stress-strain behavior. *Soil Mechanics*, John Wiley & Sons, 122-136.
- Masaharu, H., Hasegawa, H., Ohtsubo, K. (2001): Three-dimensional city modeling from airborne laser scanning, Proceedings of the 20th International Cartographic Conference, International Cartographic Association, 2, pp. 1337-1343.
- Mogami, T. (1969): Soil mechanics. Gihoudo, 1048 pp (In Japanese).
- Moriwaki, H. (1993): Behavior of pore-water pressure at slope failure. Proceedings of the seventh International Conference and Field Workshop on Landslides in Czech and Slovak Republics, "LANDSLIDES". A.A.Balkema, Rotterdam, pp263-268.
- Moriwaki, H. (2001): A risk evaluation of landslides in use of critical surface displacement. *Landslide - Journal of the Japan Landslide Society*, 38(2):115-127 (In Japanese with English abstract).
- Moriwaki, H. and Sato, T. (1998): Motion and Fluidization of a Hariharagawa Landslide, South Japan. Proceedings of International Union of Forest Research Organization 8 Conference, Environmental Forest Science, Kluwer Academic Publishers, pp569-574.
- Moriwaki, H., Inokuchi, T., Hattanji, T., Sassa, K., Ochiai, H. and Wang, G. (2004): Failure processes in a full-scale landslide experiment using a rainfall simulator. *Landslides*, Vol.1, No.4, pp.277 - 288.
- Noguchi, S., Abdul Rahim N., Zulkifli, Y., Tani, M., Sammori, T. (1997): Soil physical properties and preferential flow pathways in tropical rain forest, Bukit Tarek, Peninsular Malaysia. *Journal of Forest Research*, 2: 125-132.
- Ochiai, H., Okada, Y., Furuya, G., Okura, Y., Matsui, T., Sammori, T., Terajima, T. and Sassa, K. (2004): A fluidized landslide on a natural slope by artificial rainfall, *Landslides*, Vol.1, No.3, pp.211-219.
- Oka, H. (1972): Impacts by the "artificial landslide":re-examine the rage of nature. *Kagaku Asahi*, January issue:152-153. (in Japanese).
- Oka, S. (1991): Geology of Middle-Upper Pleistocene series in southwestern Kanto district. *Bulletin of Geological Survey of Japan*, 42: 553-653 (in Japanese).
- Okuda, S. (1984): Features of debris deposits of large slope failures investigated from historical records. Annual report of Disaster Prevention Research Institute, Kyoto University, No.27 B-1, 353-368 (In Japanese with English abstract).
- Okura, Y., Kitahara, H., Ochiai, H., Sammori, T., Kawanami, T. (2002): Landslide fluidization process by flume experiment. *Engineering Geology* 66, 65-78.
- Reid, M.E., Lahusen, R.G., Iverson, R.M. (1997): Debris-flow initiation experiments using diverse hydrologic triggers. Proceedings of the ASCE First International Conference on Debris-Flow Hazards Mitigation: Mechanics, Prediction, and Assessment. 1-11.
- Sassa, K. (1984): The mechanism starting liquefied landslides and debris flows. In Proceedings of the 4th International Symposium on Landslides, Toronto, 16 21 September, 2, 349-354.
- Sassa, K. (1985): The mechanism of debris flow. Proceedings of 11th International Conference on Soil Mechanics and Foundation Engineering, San Francisco, Balkema, Rotterdam, Vol 3, pp 1173-1176.

- Sassa, K. (1988a): Motion of landslides and debris flows -prediction of hazard area-, Report for Grant-in-Aid for Scientific Research by Japanese Ministry on Education, Science and Culture (Project No. 61480062), 4-52.
- Sassa, K. (1988b): Special Lecture: The geotechnical model for the motion of landslides. Proc. 5th International Symposium on Landslides, Lausanne, Vol.1, pp 33-52.
- Sassa, K. (1994): Development of a new cyclic loading ring shear apparatus to study earthquake-induced landslides. Report for Grant-in-Aid for Developmental Scientific Research by the Japanese Government. Project No. 03556021.
- Sassa, K. (1995): Access to the dynamics of landslides during earthquakes by a new cyclic loading ring shear apparatus. Proc. for 6th International Symposium on Landslides, Landslides, Balkema, Rotterdam, Vol 1, pp 1919-1939.
- Sassa, K. (1996): Prediction of earthquake induced landslides. Proceedings of 7th International Symposium on Landslides, A.A. Balkema, Rotterdam, The Netherlands, Vol 1, pp 115-132.
- Sassa, K., Fukuoka, H., Scarascia-Mugnozza, G. and Evans, S.G. (1996): Earthquake-induced- landslides: Distribution, motion and mechanisms. Soils and Foundations, Special Issue, 53-64.
- Sassa, K., Fukuoka, H., Wang, F.W. (1997): Mechanism and risk assessment of landslide- triggered-debris flows: lesson from the 1996.12.6 Otari debris flow disaster, Nagano, Japan. D.M. Cruden & R. Fell, eds. Landslide Risk Assessment, Proceedings of the international workshop on landslide risk assessment. Honolulu, 19-21 February, 347-356.
- Sassa, K. (1998a): Mechanisms of landslide triggered debris flows. Environmental Forest Science, In Proceedings of IUFRO Division 8 Conference, Kyoto, 19 - 23 October, 499-518.
- Sassa, K. (1998b): Mechanisms of landslide triggered Debris flows. Keynote Lecture for the IUFRO (International Union of Forestry Research Organization) Division 8 Conference, Environmental Forest Science, Forestry Science, Kluwer Academic Publishers, 54:499-518.
- Sassa, K. (2000): Mechanism of flows in granular soils. Proceedings of GeoEng2000, Melbourne, Vol 1, pp 1671-1702.
- Sassa, K. (2002): Study on the mechanism of earthquake and rainfall induced rapid flow phenomena- Disasters and their mitigation in large-scale cities. Proceedings of the symposium on Aerial Predictions of Earthquake and Rainfall Induced Flow Phenomena (APERIF), "New century of urban area landslides disaster mitigation", Tokyo (in Japanese). 31 August-1 September 2002, pp. 7-33.
- Sassa, K., Wang, G. and Fukuoka, H. (2003): Assessment, of earthquake-induced catastrophic landslides in urban areas and their prevention planning. Proceedings of International Conference on Slope Engineering, December 2003, the University of Hong Kong, Vol 1, pp. 26-49.
- Sassa, K., Wang, G. and Fukuoka, H. (2003): Performing undrained shear tests on saturated sands in a new intelligent type of ring shear apparatus. Geotechnical Testing Journal, 26(3):257-265.
- Sassa, K., Fukuoka, H., Wang, G. and Ishikawa, N. (2004a): Undrained dynamic-loading ring-shear apparatus and application for landslide dynamics. Landslides 1(1): 7-19.
- Sassa, K. (2004b): Preface. Landslides, Vol.1, No.3, pp.169 - 171.
- Sassa, K., Wang, G., Fukuoka, H., Wang, F., Ochiai, T., Sugiyama, M. and Sekiguchi, T. (2004c): Landslide risk evaluation and hazard zoning for rapid and long-travel landslides in urban development areas. Landslides, Vol.1, No.3, pp.221 - 235.
- Sato, H.P., Hasegawa, H., Okamatsu, K. and Masaharu, H. (2002): Landslide Topography Measurement by Airborne Laser Scanning. Proceedings of international symposium on Landslide Risk Mitigation and Protection of Cultural and Natural Heritage, pp. 375-383, UNESCO and Kyoto University.
- Seed, H.B. (1979): Soil liquefaction and cyclic mobility evaluation for level ground during earthquakes. Journal of the Geotechnical Engineering Division, ASCE, 105: 201-255.
- Seed, H.B. and Lee, K.L. (1966): Liquefaction of saturated sand during cyclic loading. Journal of the Geotechnical Engineering Division, ASCE, 92(CM6): 105-134.
- Sekiguchi, T., Fukushima, Y. and Nemoto, T. (1996): Mapping of earthquake damage caused by the Southern Hyougo Prefectural Earthquake of 1996, Geographical Review of Japan, Vol 69A-7, pp. 579-594 (in Japanese).
- Sekiguchi, T., Sato, H.P., Ichikawa, S. and Kojiroi, R. (2003): Mapping of micro topography on hill slopes

- using airborne laser scanning, Bulletin of Geographical Survey Institute, 49, pp. 47-57.
- Sekiguchi, T. and Sato, H.P. (2004): Mapping of micro topography using airborne laser scanning. Landslides, Vol.1, No.3, pp.195 - 202.
- Spence, K.J. and Guymer, I. (1997): Small-scale laboratory flowslides. Geotechnique 47(5): 915-932.
- Takahashi, T. (1991): Debris Flow. Rotterdam: Balkema. 165pp.
- Unozawa, A. and Oka, S. (1972): 1:10,000 Geological map of Kanto loam beds in north western part of Tama Hill, Geological Survey of Japan (in Japanese).
- Wang, G. and Sassa, K. (2002): Pore pressure generation and motion of rainfall-induced landslides in laboratory flume tests. Proceedings of International Symposium on Landslide Risk Mitigation and Protection of Cultural and Natural Heritage, UNESCO and Kyoto University, pp. 45-60.
- Wang, G. and Sassa, K. (2003): Pore-pressure generation and movement of rainfall-induced landslides: effects of grain size and fine-particle content. Engineering Geology 69:109-125.
- Wehr, A. and Lohr, U. (1999): Airborne laser scanning an introduction and overview, ISPRS Journal of Photogrammetry and Remote Sensing, 54: 68-82.
- Yagi, N., Yatabe, R. and Enoki, M. (1985): Laboratory and field experiments on prediction method of occurring time of slope failure due to rainfall. Landslide - Journal of Japan Landslide Society 22(2):1-7 (In Japanese with English abstract).
- Yamaguchi, I., Nishio, K., Kawabe, H., Shibano, H. and Iida, C. (1989): Initiation and fluidization of an artificial landslide. -Field experiment in Yui, Shizuoka Prefecture, Japan-, Shinrin Kosoku(Areal Survey) 158, 3-9. (in Japanese).
- Yoshimi, Y., Richart, F.E., Prakash, S., Balkan, D.D. and Ilyichev, V.A. (1977): Soil dynamics and its application to foundation engineering. In Proceedings of the 9th International Conference on Soil Mechanics and Foundation Engineering, Tokyo, July, 2, 605-650.

地震豪雨時の高速長距離土砂流動現象の解明(APERITIF)プロジェクトの成果

佐々恭二・福岡 浩・関口辰夫*・森脇 寛**・落合博貴***

*国土交通省国土地理院

**独立行政法人防災科学技術研究所

***独立行政法人森林総合研究所

要旨

都市域の住宅密集地における地震時高速長距離地すべりの危険度評価は世界中の地すべり危険地帯のどこにおいても現在もっとも重要な災害軽減における課題となっている。本報では佐々が代表を務める地震豪雨時の高速長距離土砂流動現象の解明(APERITIF)プロジェクトのうち、重要な成果をとりあげ紹介する。具体的には、(1)空中レーザースキャンによる地すべり危険地形の抽出、(2)人工降雨装置を用いた実規模斜面モデルによる実験、(3)自然斜面における人工降雨による地すべり発生実験、(4)都市化域における地すべり危険度評価と災害危険地区予測、の4課題について紹介する。(4)の試験地は東京近郊の多摩地区の住宅密集地2カ所に設定され、現地調査、地質ボーリング、レーザースキャン型高度計による測量、リングせん断試験など室内実験の結果をあわせたところ、両試験地においてすべり面液状化の可能性があることを示した。本研究において得られた定量的なデータを用いた地盤工学的地すべり運動シミュレーション(RAPIDLS)により、都市域における地すべり危険値予測を街区単位で実現することができた。

キーワード: 危険度評価, ハザードゾーニング, 地震時地すべり, 流動化, 航空レーザースキャナー, フルスケール土槽試験, 自然斜面, 間隙水圧, すべり面形成, 非排水リングせん断試験, 数値シミュレーション